Journal of the Korean Physical Society, Vol. 69, No. 12, December 2016, pp. 1817∼1823

Deviations from Stoichiometry and Molecularity in Non-Stoichiometric Ag-In-Se Thin Films: Effects on the Optical and the Electrical Properties

Nam-Hoon Kim, Myoung Han Yoo, Pil Ju Ko and Woo-Sun Lee*
Department of Electrical Engineering, Chosun University, Gwangju 61452, Korea

(Received 21 October 2016, in final form 8 November 2016)

Non-stoichiometric Ag-In-Se (AIS) thin films were prepared using co-sputtering with $InSe_2$ and Ag targets followed by rapid thermal annealing. The internal stress of the non-stoichiometric AIS thin films was strongly affected by the deviation from molecularity, Δm. When Δm was far from stoichiometry, the non-stoichiometric AIS thin films showed better crystallinity. The improvement in the crystallinity and the release of internal stress led to a reduction in the optical band gap from 1.63 to 1.19 eV and in the resistivity from 6.45×10^{-2} to 3.21×10^{-3} Ω·cm for the non-stoichiometric AIS thin films, with a similar tendency for the deviation from molecularity, Δm. The non-stoichiometric AIS thin films, with $\Delta m < 0$ and $\Delta s < 0$, exhibited n-type conductivity with carrier concentrations on the order of magnitude of 10^{18} cm^{-3}. The mean absorbance of the 200-nm-thick non-stoichiometric AIS thin films was 1.50, corresponding to an absorption of approximately 96.84 % of the incident light in the visible region.

PACS numbers: 85.60.Bt, 85.40.Sz
Keywords: AIS thin film, Non-stoichiometric, Deviation from molecularity Δm
DOI: 10.3938/jkps.69.1817

I. INTRODUCTION

The A^I-B^{III}-C^{VI} ternary chalcopyrite Ag-In-Se (AIS) has a direct band gap (∼1.2 eV) and a large optical absorption coefficient ($> 10^4$ cm^{-1}) [1, 2]. AIS is one of the potential candidates for use in many applications such as photovoltaic cells, near-infrared (NIR) optical devices, nonlinear optical devices, ligh-emitting diodes (LEDs), Schottky diodes, and thermoelectric power generation [3, 4]. The optical band gap (E_g) of AIS thin films can be varied from 1.18 to 1.42 eV with either n- or p-type conductivity by changing the preparation and the post-treatment methods [5–7]. Various methods have been used to prepare AIS thin films, including flash evaporation, RF magnetron sputtering, thermal evaporation, solution growth, electro-deposition, co-evaporation, horizontal Bridgman method, molecular beam epitaxy, solid state microwave irradiation, vertical gradient temperature freezing method, and pulsed laser deposition (PLD) [7–9].

In this study, AIS thin films were prepared by using a co-sputtering process with Ag and $InSe_2$ targets, followed by rapid thermal annealing (RTA). Controlling the stoichiometry of the ternary indium selenides is usually difficult because Se is known to have high volatility during high-temperature synthesis for a long time [8,10,11]. Therefore, the influence of the various compositions in the AIS thin films on the characteristics by minimizing the volatility of Se during the preparation of AIS thin films should be investigated. The microstructure and the electrical and the optical properties of the AIS thin films with different compositions caused by the deposition conditions were examined.

II. EXPERIMENTAL DETAILS

AIS thin films, approximately 200 nm in thickness, were deposited on Corning glass (20×20 mm^2) substrates by using RF magnetron co-sputtering (IDT Engineering Co.) with commercial $InSe_2$ (LTS Chemical Inc., 99.99 % purity, diameter: 50.8 mm) and Ag (LTS Chemical Inc., 99.999 % purity, diameter: 50.8 mm) targets. The process parameters were set as follows: pre-sputtering for 3 min, a substrate-to-target distance of 5.0 cm, an Ar gas flux of 50 sccm, a base pressure of 1.0×10^{-6} Torr, and a vacuum pressure of 7.5×10^{-3} Torr at room temperature. The chemical composition of the AIS thin films was controlled by regulating the RF power of the Ag target. The RF power for Ag was set to 15, 17, 19, 21, and 23 W for different samples by using sputtering times of 765, 715, 660, 610, and 560 s, respectively, to maintain a total thickness of approximately 200 nm when the RF power for $InSe_2$ was fixed at 30 W with

*E-mail: wslee@chosun.ac.kr

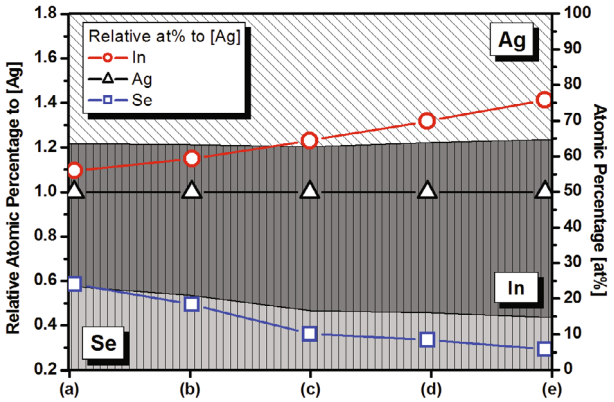

Fig. 1. (Color online) Chemical compositions of the RTA-treated AIS thin films at sputtering powers of (a) 15, (b) 17, (c) 19, (d) 21, and (e) 23 W for the Ag target with a fixed power of 30 W for the $InSe_2$ target. The corresponding co-sputtering times were 765, 715, 660, 610, and 560 s, respectively.

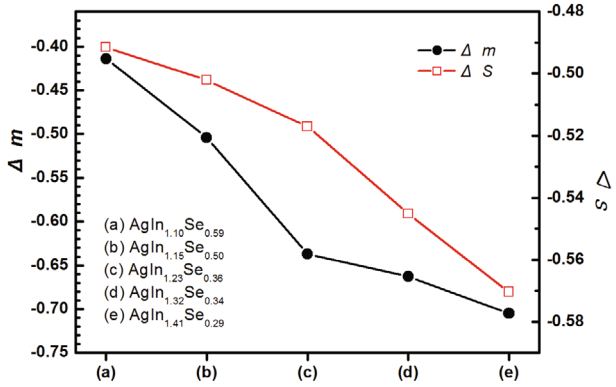

Fig. 2. (Color online) Deviation parameters Δm = [Ag]/[In] − 1 and Δs = 2[Se]/([Ag]+3[In]) − 1 derived from the chemical compositions of the non-stoichiometric AIS thin films at (a) $AgIn_{1.10}Se_{0.59}$, (b) $AgIn_{1.15}Se_{0.50}$, (c) $AgIn_{1.23}Se_{0.36}$, (d) $AgIn_{1.32}Se_{0.34}$, and (e) $AgIn_{1.41}Se_{0.29}$.

a deposition rate of 12.0 nm/min. The individual deposition rates of Ag for these process parameters were 3.69, 4.78, 6.18, 7.67, and 9.43 nm/min at 15, 17, 19, 21, and 23 W RF power, respectively. RTA (GD-TECH Co., GRT-100) of the 200-nm-thick thin films was performed at 400 °C for 10 min under N_2 gas to reduce the volatilization of Se from the thin films by using a short process time and decreased thermal exposure [11,12].

The crystalline structure of the AIS thin films was analyzed using X-ray diffraction (XRD, PANalytical X'pert PRO MRD) at 40 kV and 30 mA with Cu Kα X-ray source (λ = 0.15406 nm) over the 2θ range of 10 - 90°. An energy-dispersive X-ray spectroscope (EDX, Oxford Instruments, INCA), attached to a field-emission scanning electron microscope (FESEM, JEOL, JSM-7500F), was used for analyzing the chemical composition of each element in the AIS thin films. The optical properties of the AIS thin-films were characterized using an ultraviolet-visible spectrophotometer (BaySpec Inc., UNIR-230) over the range of 400 - 1500 nm. The electrical properties of the AIS thin films, including the resistivity, carrier concentration, and mobility, were measured using a Hall-effect measurement system (Accent Optical Technologies, HL5500PC) at room temperature.

III. RESULTS AND DISCUSSION

The chemical compositions of the RTA-treated AIS thin films were examined by using an EDX, and the results are shown in Fig. 1. The Ag content was controlled by adjusting the individual thickness in the films by varying the RF power for each target in the co-sputtering process. The RF powers for the Ag target were (a) 15, (b) 17, (c) 19, (d) 21, and (e) 23 W for sputtering times of 765, 715, 660, 610, and 560 s, respectively, with a fixed RF power for the $InSe_2$ target in order to increase the Ag content in the AIS thin films at the maintained total thickness. However, the atomic percentages of the AIS thin films did not depend on the thickness ratio in the co-sputtering process [13–15], as shown in Fig. 1. The atomic percentage of Ag remained relatively constant with increasing RF power for the Ag target while the atomic percentage of In increased gradually as the atomic percentage of Se decreased rapidly. For the shorter deposition times, Se is not only more volatile but also more difficult to deposit than In in the In-Se interlayer [16, 17]. Hence, the conditions were re-defined by varying the compositional ratios of In and Se with a fixed Ag content in the non-stoichiometric AIS thin films, such as (a) $AgIn_{1.10}Se_{0.59}$, (b) $AgIn_{1.15}Se_{0.50}$, (c) $AgIn_{1.23}Se_{0.36}$, (d) $AgIn_{1.32}Se_{0.34}$, and (e) $AgIn_{1.41}Se_{0.29}$, with the AIS thin film being near-stoichiometric at $Ag_{1-x}In_{1-3x}Se_{2(1+3x)}$, where $x \leq 0.045$ [4].

Two parameters Δm and Δs were examined to survey the deviations from molecularity and stoichiometry, respectively: Δm = [Ag]/[In] − 1 and Δs = 2[Se]/([Ag]+3[In]) − 1 [18–20]. In the case of stoichiometric compounds, the parameters exhibited no deviation. Figure 2 shows the Δm and the Δs in the non-stoichiometric AIS thin films for various compositional ratios of In and Se with a fixed Ag content. Ag-poor ($\Delta m < 0$) and Se-poor ($\Delta s < 0$) compositions were obtained in all the specimens. As the In content was increased, the non-stoichiometric AIS thin films showed $\Delta m = -0.414$, -0.504, -0.637, -0.663, and -0.705. Their Δs values were -0.491, -0.502, -0.517, -0.545, and -0.570, respectively. When both Δm and Δs became far from '0' in the non-stoichiometric AIS thin film, the film was generally departing from a stoichiometric composition. In the non-stoichiometric AIS thin films deposited to attain the same thickness for a shorter deposition time, the compositional ratios show larger In contents and lower Se contents at fixed Ag content; then, both Δm and Δs

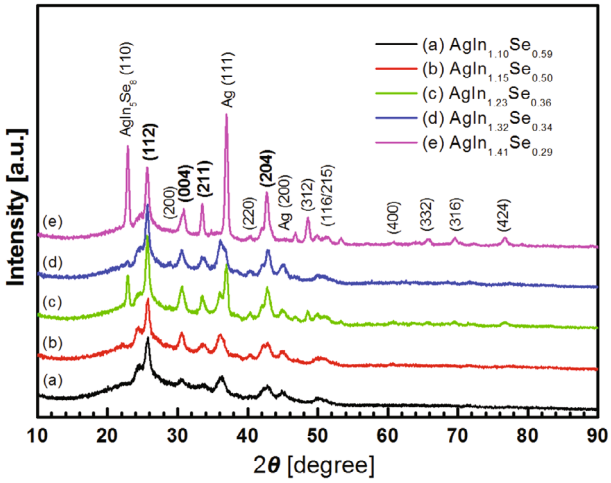

Fig. 3. (Color online) XRD patterns of the non-stoichiometric AIS thin films with different compositions (a) $AgIn_{1.10}Se_{0.59}$, (b) $AgIn_{1.15}Se_{0.50}$, (c) $AgIn_{1.23}Se_{0.36}$, (d) $AgIn_{1.32}Se_{0.34}$, and (e) $AgIn_{1.41}Se_{0.29}$.

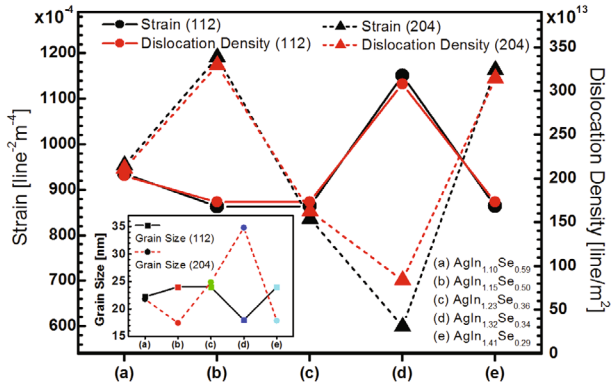

Fig. 4. (Color online) Strain and dislocation density of the non-stoichiometric AIS thin films with different compositions: (a) $AgIn_{1.10}Se_{0.59}$, (b) $AgIn_{1.15}Se_{0.50}$, (c) $AgIn_{1.23}Se_{0.36}$, (d) $AgIn_{1.32}Se_{0.34}$, and (e) $AgIn_{1.41}Se_{0.29}$. The inset shows the grain sizes in the non-stoichiometric AIS thin films under the same conditions

are farther from the value for a near-stoichiometric composition.

The XRD patterns of the non-stoichiometric AIS thin films with different compositional ratios with increasing In content and decreasing Se content at a fixed Ag content were obtained over the 2θ range of 10 - 90°, and the results are shown in Fig. 3. The non-stoichiometric AIS thin films showed major diffraction peaks corresponding to the AIS chalcopyrite phases with the preferred orientations of (112), (004), (211), and (204) at $2\theta = 25.77°$, 30.58°, 33.49°, and 42.77°, respectively, as shown in Fig. 3 [2, 4, 9]. Some weak peaks were also observed in the specimens at $2\theta = 28.81°$, 40.46°, 51.17°, 60.87°, 65.94°, 69.63°, and 76.78° corresponding to the positions of the (200), (220), (116)/(215), (400), (332), (316), and (424) peaks [9]. The observation of the weak peaks in the XRD patterns means that small grains were formed and that insufficient grain growth occurred along the orientations not shown in Fig. 3. The peaks at $2\theta = 37.00°$ and 45.04° are those of the unreacted Ag which the strong peak at $2\theta = 22.91°$ corresponds to $AgIn_5Se_8$ in the specimens in (c) $AgIn_{1.23}Se_{0.36}$ and (e) $AgIn_{1.41}Se_{0.29}$, which indicates that the specimens are not of good quality [9]. Moreover, the peak corresponding to the (112) orientation shifted to lower 2θ values from 25.77° for the compositions (a) $AgIn_{1.10}Se_{0.59}$ and (b) $AgIn_{1.15}Se_{0.50}$ to 25.67° for the composition (d) $AgIn_{1.32}Se_{0.34}$ and to 25.64° for the compositions (c) $AgIn_{1.23}Se_{0.36}$ and (e) $AgIn_{1.41}Se_{0.29}$. This is consistent with the typical shift in the diffraction pattern to lower angles with increasing In or Se content due to increase in the 'a' and the 'c' lattice constants [21–23]. The d spacing decreased as more of the larger In or Se atoms were added to the normal AIS lattice. Therefore, XRD suggests that polycrystalline AIS was rebuilt on the substrate and that the crystal quality could be modified by changing the In or the Se content in the co-sputtering process. However, in this study, the composition ratio of the non-stoichiometric AIS thin films changed with an increase in the In content and a simultaneous decrease in the Se content.

The strain (ε) and the dislocation density (δ) were calculated by using the equations $\varepsilon = \omega \cos\theta/4$ and $\delta = 1/D^2$, respectively, where ω is the full width at half maximum (FWHM) of the preferred diffraction peak, θ is the angle corresponding to the preferred reflection and D is the mean grain size of the crystallites in the non-stoichiometric AIS thin films [24–26]. The strain and the dislocation density were calculated using both the preferred (112) and (204) peaks. The strain along the (112) direction gradually decreased with an increase in the In content and a simultaneous decrease in the Se content, but the strain in the non-stoichiometric AIS thin films increased for the composition (d) $AgIn_{1.32}Se_{0.34}$, as shown in Fig. 4. The strain along the (204) direction increased and decreased for the compositions (b) $AgIn_{1.15}Se_{0.50}$ and (d) $AgIn_{1.32}Se_{0.34}$, respectively. The increase in the strain is strongly involved in introducing crystalline defects, such as dislocations and stacking faults, in the crystal [27–29]. The non-stoichiometric AIS thin films grew greater along the (204) direction with a decrease in the strain/stress for the composition (d) $AgIn_{1.32}Se_{0.34}$ whereas the AIS thin films were highly oriented along the (112) direction for the compositions (b) $AgIn_{1.15}Se_{0.50}$ and (e) $AgIn_{1.41}Se_{0.29}$. This result agreed with the opposite trends for the grain size along the directions (the inset of Fig. 4), which was calculated using the Debye-Scherrer formula $D = 0.94\lambda/\omega\cos\theta$, where λ is the wavelength of the Kα radiation of Cu ($\lambda = 0.15406$ nm), ω is the FWHM of each diffraction peak and θ is the angle corresponding to each reflection [30–32]. The dislocation density, defined as the length of the dislocating lines per unit volume of the crystal [33], showed a tendency similar to the strain along each direction. The lowest dislocation

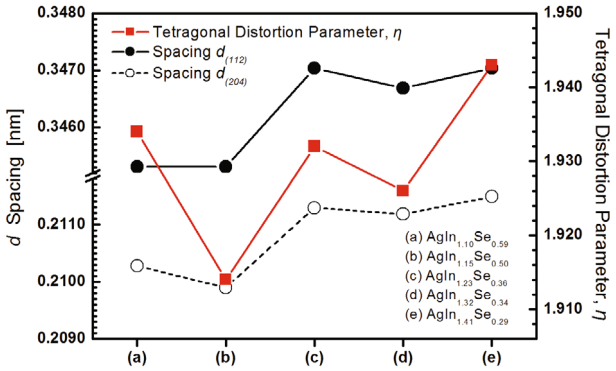

Fig. 5. (Color online) Distortion parameter η and inter-planar d spacing of the non-stoichiometric AIS thin films with different compositions: (a) $AgIn_{1.10}Se_{0.59}$, (b) $AgIn_{1.15}Se_{0.50}$, (c) $AgIn_{1.23}Se_{0.36}$, (d) $AgIn_{1.32}Se_{0.34}$, and (e) $AgIn_{1.41}Se_{0.29}$.

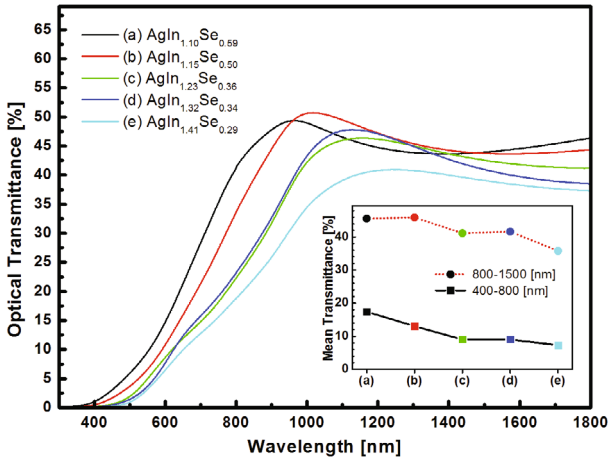

Fig. 6. (Color online) Optical transmittances of the non-stoichiometric AIS thin films with different compositions: (a) $AgIn_{1.10}Se_{0.59}$, (b) $AgIn_{1.15}Se_{0.50}$, (c) $AgIn_{1.23}Se_{0.36}$, (d) $AgIn_{1.32}Se_{0.34}$, and (e) $AgIn_{1.41}Se_{0.29}$. The inset shows the mean optical transmittance in the visible (400 - 800 nm) to the NIR (800 - 1500 nm) spectral region under the same conditions.

densities of 17.31×10^{13} and 8.24×10^{13} line/m^{-2} were observed for the compositions (e) $AgIn_{1.41}Se_{0.29}$ and (d) $AgIn_{1.32}Se_{0.34}$ along the (112) and the (204) directions, respectively, which indicates that the lowest lattice mismatch was obtained under these conditions with a release of strain [34,35].

The lattice constants a and c were calculated using the equation $1/d^2 = (h^2 + k^2)/a^2 + l^2/c^2$ combined with Bragg's law $d = \lambda/2\sin\theta$ in the tetragonal structure. In both equations, hkl are the Miller indices, d is the inter-planar spacing in the atomic lattice, θ is the angle between the incident ray and the scattering planes, and λ is the wavelength of the Cu Kα radiation ($\lambda = 0.15406$ nm) [4, 9, 34]., The d spacing can be determined using Bragg's law for a particular incident X-ray wavelength, λ, and angle, θ, from XRD. The lattice constants a and c can be simultaneously calculated using the (112), (004), (211) and (204) peaks. The lattice constants were in the range a = 0.6050 - 0.6088 and c = 1.1620 - 1.1795 nm. The tetragonal distortion parameter in the non-stoichiometric AIS thin films for different compositional ratios, $\eta = c/a$, was also in the range of 1.914 - 1.943, as shown in Fig. 5. These values are in good agreement with the values reported for most chalcopyrite tetragonal crystals [4, 9, 36, 37]. The distortion parameter of the non-stoichiometric AIS thin-film was affected by the compositional ratios of the thin films themselves, with a similar tendency for the normalized value of Δm (Fig. 2). The inter-planar spacing of the (112) and the (204) peaks ($d_{(112)}$ and $d_{(204)}$), determined from the peak positions of each sample, in the non-stoichiometric AIS thin films at different compositional ratios were calculated using Bragg's law, and the results are shown in Fig. 5, which showed a similar trend of increasing slightly and showing a 'W' shape with further addition of larger In atoms to and removal of larger Se atoms from the AIS lattice, generally indicating better crystallinity because of the decrease in the number of structural defects and internal stresses [20]. Determining whether if the increasing trend of the d spacing can be attributed to the increase in the In content or the decrease in the Se content in the non-stoichiometric AIS thin films is difficult. Note that both the $d_{(112)}$ and the $d_{(204)}$ values showed an opposite trend for Se (Fig. 1) and/or a similar trend for the normalized value of Δm (Fig. 2).

Figure 6 shows the optical transmittance in the visible to the NIR spectral region for the non-stoichiometric AIS thin films. All the spectra showed optical transmittances of $\leq$ 42 % in the visible region (400 - 800 nm), and the mean optical transmittance was $\leq$ 18 % over the same wavelength range. The mean optical transmittance of the non-stoichiometric AIS thin films was 7.29 % for the composition $AgIn_{1.41}Se_{0.29}$ (Fig. 6(e)). This was somewhat lower than the mean optical transmittances for the specimens with relatively lower In content (17.42 % at $AgIn_{1.10}Se_{0.59}$), as shown in Fig. 6(a). The mean optical transmittance showed a tendency to decrease with increasing In content. The non-stoichiometric AIS thin films showed considerable absorption in the visible region. All the optical transmittances converged to zero regardless of the In content. The Burstein-Moss (B-M) shift was also observed with increasing In content. The B-M shift is a shift of the absorption edge to a larger wavelength. This highlights the advantages of using non-stoichiometric AIS thin films as the absorber layer in thin-film solar cells, *i.e.*, the decrease in the spectral transmission range for the minimum in the solar emission spectrum [38–40]. The observation of the B-M shift means that the advantage of using AIS thin films as absorber layers was caused by an increase in the In content. The absorption coefficients (α) of the non-stoichiometric AIS thin films were calculated using Beer-Lambert's law in the high absorption region [41,42]: $\alpha(\nu) = (2.303/d)A$,

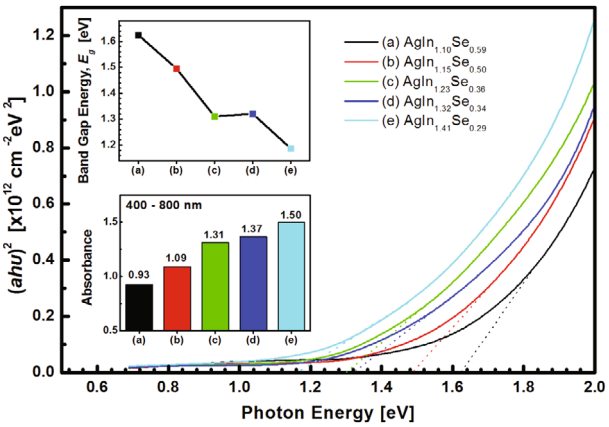

Fig. 7. (Color online) Tauc plots of $(\alpha h\nu)^2$ vs. photon energy ($h\nu$) for the non-stoichiometric AIS thin films with different compositions: (a) $AgIn_{1.10}Se_{0.59}$, (b) $AgIn_{1.15}Se_{0.50}$, (c) $AgIn_{1.23}Se_{0.36}$, (d) $AgIn_{1.32}Se_{0.34}$, and (e) $AgIn_{1.41}Se_{0.29}$. The insets show the mean absorbance in the visible (400-800 nm) spectral region and the optical band gaps (E_g) of the non-stoichiometric AIS thin films under the same conditions.

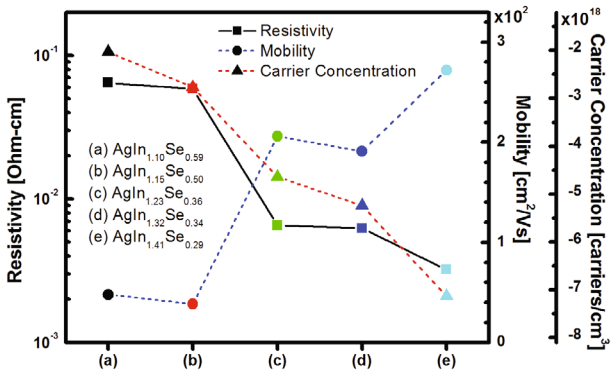

Fig. 8. (Color online) Hall-effect measurements of the resistivity (ρ), carrier concentration (n), and carrier mobility (μ) of the non-stoichiometric AIS thin films with different compositions: (a) $AgIn_{1.10}Se_{0.59}$, (b) $AgIn_{1.15}Se_{0.50}$, (c) $AgIn_{1.23}Se_{0.36}$, (d) $AgIn_{1.32}Se_{0.34}$, and (e) $AgIn_{1.41}Se_{0.29}$.

where $\alpha(\nu)$, d, and A are the absorption coefficient, the film's thickness, and the film's absorbance, respectively. The absorption coefficient is the ability of a semiconductor to absorb photons, *i.e.*, a measure of how far below the surface of the AIS thin film an incident photon of a particular wavelength is absorbed [43, 44]. This can be expressed as $\alpha = (1/d)\ln[(1-R)/T]$, where T, d, and R are the optical transmittance, reflectance, and film's thickness, respectively [45]. The absorption coefficient of the AIS thin film was high (approximately 10^5 cm^{-1}) in the visible region; however, it was somewhat lower (approximately 10^4 cm^{-1}) in the NIR region (not shown). The absorption coefficients of the non-stoichiometric AIS thin films with the same thicknesses were directly affected by the optical transmittance. The lower optical transmittance of the non-stoichiometric AIS thin films with an increased defect density caused by an increase in In and a simultaneous decrease in Se to the normal AIS lattice is thought to be attributed to more phonon scattering and is thought to prevent incident visible light from being transmitted through the non-stoichiometric AIS thin film in the visible region [46].

The absorbance was calculated using the following formula: $A = -\log T = \log(I_0/I)$, where A is the absorbance, T is the transmittance, I_0 is the intensity of incident radiation and I is the intensity of the transmitted radiation at a given wavelength. The absorbance of the non-stoichiometric AIS thin films showed mean values over the 400- to 800-nm range. The mean absorbance for the lower composition of In content at (a) $AgIn_{1.10}Se_{0.59}$ thin film was in 0.93, which means that approximately 88.25 % of the incident photons in the 400- to 800-nm range are absorbed by these approximately 200-nm-thick non-stoichiometric AIS thin films. The mean absorbance was enhanced by increasing In and simultaneously decreasing Se, as shown in the inset of Fig. 7. The maximum mean absorbance value of the non-stoichiometric AIS thin films was 1.50 for the (e) $AgIn_{1.41}Se_{0.29}$ thin film, which suggested that approximately 96.84 % of the incident photons in the visible region were absorbed by these non-stoichiometric AIS thin films. The optical band gap of the non-stoichiometric AIS thin films was estimated by linearly extrapolating each of the Tauc plots of $(\alpha h\nu)^2$ vs. the photon energy ($h\nu$) back to the energy axis, as shown in Fig. 7, where α is the absorption coefficient, h is Planck's constant, and ν is the frequency of the incident photon. The optical band gaps of the non-stoichiometric AIS thin films were in the range 1.19 - 1.63 eV. Note that the optical band gaps of the non-stoichiometric AIS thin film showed a similar tendencies for Δm (Fig. 2) and the Se composition (Fig. 1). The optical band gap is attributed to both the crystallinity and the intrinsic defects that cause a shift in the absorption edge [47]. Higher crystallinity leads to a decrease in the optical band gap because a lower free-carrier concentration and lower potential barriers originated from large particles with fewer grain boundaries and imperfections [48].

Hall-effect measurements were performed to examine the electrical properties, such as the conductivity type, resistivity, carrier concentration, and carrier mobility, of the non-stoichiometric AIS thin films with increasing In content and simultaneously decreasing Se content in relation to the In target's sputtering power, and the results are shown in Fig. 8. The Hall-effect measurements showed n-type conductivity in all the non-stoichiometric AIS thin films with $\Delta m < 0$ (In-rich) and $\Delta s < 0$ (Se-deficient), as shown in Fig. 2. The conductivity type of Cu-In-Se single crystals was determined by the deviations [49], and the Cu-In-Se thin films with $\Delta m < 0$ and $\Delta s < 0$ always had n-type conductivity [19]. A systematic study is necessary to apply the relationship to the AIS thin films. The carrier concentration of the

non-stoichiometric AIS thin films were on the order of magnitude of 10^{18} cm^{-3} excess electrons because they had n-type conductivity and their carrier mobility varied from 38.5 to 272.0 $cm^2 \cdot V^{-1}s^{-1}$, which is in close agreement with previously reported values for AIS thin films [50]. The increased carrier concentration, with the carriers acting as donors in n-type AIS thin films, can lead to a decreased band gap in the AIS thin films. This would allow more efficient harvesting of incident light at larger wavelengths. The resistivities of the non-stoichiometric AIS thin films were on the order of 10^{-3} - 10^{-2} Ω·cm. The resistivity of a thin film generally depends on the carrier concentration and the carrier mobility, which is similar to the trend for Δm (Fig. 2) and the normalized value of Δm (Fig. 5), respectively. The decreased resistivity of the non-stoichiometric AIS thin films was attributed to the reduced grain boundaries because the improved crystallinity decreased the scattering of charge carriers and subsequently decreased the resistivity, with increasing In content. The reduced resistivity would affect the improvement of the short-circuit current density and fill factor of the solar cell because of the decreased series resistance of the thin films.

IV. CONCLUSION

AIS thin films were treated with RTA in a N_2 ambient following co-sputtering with Ag and $InSe_2$ targets. The chemical composition of the AIS thin films did not depend on the thickness ratio in the co-sputtering process, and the thin films were obtained with varying ratios of the In and Se content in the non-stoichiometric AIS thin films. The deviations from molecularity and stoichiometry, Δm and Δs, respectively, in the non-stoichiometric AIS thin films were examined, and the results showed that all the specimens were In-rich ($\Delta m < 0$) and Se-deficient ($\Delta s < 0$). The internal stress, including the distortion parameter and the d spacing, of the non-stoichiometric AIS thin film was strongly related to the deviation from molecularity, Δm. When both Δm and Δs became far from the stoichiometric composition in the AIS thin film, the crystallinity became better because of the reduced number of structural defects and the reduced internal stresses. The better crystallinity and the released intrinsic defects led to decreases in the optical band gap and the resistivity of the non-stoichiometric AIS thin films. The optical band gaps of the non-stoichiometric AIS thin films were in the range of 1.19 - 1.63 eV, showing a similar tendency for the deviation from molecularity, Δm. The mean absorbance value of the non-stoichiometric AIS thin films was 1.50, suggesting that approximately 96.84 % of the incident photons in the visible region were absorbed by these non-stoichiometric AIS thin films. The carrier concentration was on the order of magnitude of 10^{18} cm^{-3} excess electrons of n-type conductivity at deviations of $\Delta m < 0$ and $\Delta s < 0$ in all the non-stoichiometric AIS thin films. The resistivities of the non-stoichiometric AIS thin films were in the range from 10^{-3} to 10^{-2} Ω·cm.

ACKNOWLEDGMENTS

This study was supported by research funds from Chosun University, 2015.

REFERENCES

[1] T. Çolakoğlu and M. Parlak, J. Phys. D: Appl. Phys. **42**, 035416 (2009).
[2] M. A. Abdullaev, A. K. Akhmedov, D. Kh. Magomedova and P. P. Khokhlachev, Inorg. Mater. **48**, 987 (2012).
[3] R. Jacob, G. S. Okram, J. Naduvath, S. Mallick and R. R. Philip, J. Phys. Chem. C **119**, 5727 (2015).
[4] A. H. Ammar, A. M. Farid and M. A. M. Seyam, Vacuum **66**, 27 (2002).
[5] C. M. Joseph and C. S. Menon, Semicond. Sci. Technol. **11**, 1668 (1996).
[6] A. Ateş, M. Kundakç, A. Astam and M. Yldrm, Physica E **40**, 2709 (2008).
[7] M. A. Aouaj, R. Diaz, F. C. El Moursli, A. Tiburcio-Silver, and M. Abd-Lefdil, Int. J. Mater. Sci. Appl. **4**, 35 (2015).
[8] H. Mustafa, D. Hunter, A. K. Pradhan, U. N. Roy, Y. Cui and A. Burger, Thin Solid Films **515**, 7001 (2007).
[9] M. C. S. Kumar and B. Pradeep, Vacuum **72**, 369 (2004).
[10] K. Bouabid, A. Ihlal, A. Manar, A. Outzourhit and E. L. Ameziane, Thin Solid Films **488**, 62 (2005).
[11] N. H. Kim, Y. K. Jun and G. B. Cho, J. Electr. Eng. Technol. **9**, 1009 (2014).
[12] X. Wang, S. S. Li, W. K. Kim, S. Yoon, V. Craciun, J. M. Howard, S. Easwaran, O. Manasreh, O. D. Crisalle and T. J. Anderson, Sol. Energy Mater. Sol. Cells **90**, 2855 (2006).
[13] J. G. Lu, Z. Z. Ye, Y. J. Zeng, L. P. Zhu, L. Wang, J. Yuan, B. H. Zhao and Q. L. Liang, J. Appl. Phys. **100**, 073714 (2006).
[14] K. H. Kim, K. C. Park and D. Y. Ma, J. Appl. Phys. **81**, 7764 (1997).
[15] Y. Igasaki and H. Saito, J. Appl. Phys. **70**, 3613 (1991).
[16] F. S. Terra, G. M. Mahmoud, L. Mourad and A. Tawfik, Indian J. Phys. **86**, 1093 (2012).
[17] M. H. Yoo, Y. S. Park and N. H. Kim, J. Nanosci. Nanotech. **16**, 5128 (2016).
[18] J. Müller, J. Nowoczin and H. Schmitt, Thin Solid Films **496**, 364 (2006).
[19] S. Karthikeyan, A. E. Hill, R. D. Pilkington, J. S. Cowpe, J. Hisek and D. M. Bagnall, Thin Solid Films **519**, 3107 (2011).
[20] N. H. Kim, B. S. Sung, Y. K. Jun, D. H. Chung and W. S. Lee, J. Korean Phys. Soc. **66**, 1001 (2015).
[21] M. Venkatachalam, M. D. Kannan, S. Jayakumar, R. Balasundaraprabhu and N. Muthukumarasamy, Thin Solid Films **516**, 6848 (2008).
[22] L. P. Deshmukh, R. V. Suryawanshi, E. U. Masumdar and M. Sharon, Sol. Energy **86**, 1910 (2012).

[23] S. W. Shin, J. H. Han, Y. C. Park, G. L. Agawane, C. H. Jeong, J. H. Yun, A. V. Moholkar, J. Y Lee and J. H. Kim, J. Mater. Chem. **22**, 21727 (2012).
[24] A. Mahadkar, A. Chauhan, M. Thakurdesai and D. Gaikwad, AIP Conf. Proc. **1004**, 305 (2008).
[25] S. Neretina, N. V. Sochinskii and P. Mascher, J. Electron. Mater. **34**, 786 (2005).
[26] G. K. Williamson and R. E. Smallman, Philos. Mag. **1**, 34 (1956).
[27] D. Kim, B. Qi, D. L. Williamson and J. U. Trefny, in *IEEE 1st World Conference on Photovoltaic Energy Conversion* (Waikoloa, HI, USA, December 5-9, 2004), Vol. 1, p. 338.
[28] D. Pathak, R. K. Bedi and D. Kaur, Appl. Phys. A: Mater. **95**, 843 (2009).
[29] D. Pathak, R. K. Bedi and D. Kaur, Optoelectron. Adv. Mat. **4**, 657 (2010).
[30] J. C. Osuwa and N. I. Chigbo, Chalcogenide Lett. **9**, 501 (2009).
[31] B. D. Cullity, *Elements of X-Ray Diffraction* (3rd ed., Addison-Wesley, Reading, Mass., London, 1967).
[32] G. Gordillo, J. M. Flórez and L. C. Hernández, Sol. Energ. Mat. Sol. C. **37**, 273 (1995).
[33] S. Murugan and K. R. Murali, Acta Phys. Pol. A **126**, 727 (2014).
[34] M. A. Islam, Q. Huda, M. S. Hossain, M. M. Aliyu, M. R. Karim, K. Sopian and N. Amin, Curr. Appl. Phys. **13**, S115 (2013).
[35] J. P. Enríquez and X. Mathew, J. Mater. Sci. - Mater. El. **16**, 617 (2005).
[36] P. P. Ramesh, S. Uthanna, B. S. Naidu and P. J. Reddy, Vacuum **47**, 211 (1996).
[37] R. D. Weir, P. E. Jessop and B. K. Garside, Can. J. Phys. **65**, 1033 (1987).
[38] H. Khallaf, G. Chai, O. Lupan, L. Chow, S. Park and A. Schulte, Appl. Surf. Sci. **255**, 4129 (2009).
[39] D. S. Reddy, K. N. Rao, K. R. Gunasekhar, N. K. Reddy, K. S. Kumar and P. S. Reddy, Mater. Res. Bull. **43**, 3245 (2008).
[40] Y. Gu, X. Li, W. Yu, X. Gao, J. Zhao and C. Yang, J. Cryst. Growth **305**, 36 (2007).
[41] D. Souria and K. Shomalian, J. Non-Cryst. Solids **355**, 1597 (2009).
[42] J. M. González-Leal, A. Ledesma, A. M. Bernal-Oliva, R. Prieto-Alcón, E. Márquez, J. A. Angel and J. Cárabe, Mater. Lett. **39**, 232 (1999).
[43] S. Chandramohan, R. Sathyamoorthy, P. Sudhagar, D. Kanjilal, D. Kabiraj and K. Asokan, Thin Solid Films **516**, 5508 (2008).
[44] R. Sathyamoorthy, Sa. K. Narayandass and D. Mangalaraj, Sol. Energ. Mat. Sol. C. **76**, 339 (2003).
[45] M. S. Oh, D. K. Hwang, D. J. Seong, H. S. Hwang, S. J. Park and E. D. Kim, J. Electrochem. Soc. **155**, D599 (2008).
[46] D. H. Cho, K. S. Lee, Y. D. Chung, J. H. Kim, S. J. Park and J. Kim, Appl. Phys. Lett. **101**, 023901 (2012).
[47] S. Wageh, A. A. Higazy and M. A. Algradee, J. Mod. Phys. **2**, 913 (2011).
[48] C. V. Ramana, R. J. Smith and O. M. Hussain, Phys. Status Solidi A **199**, R4 (2003).
[49] H. Neumann and R. D. Tomlinson, Solar Cells **28**, 301 (1990).
[50] D. Abdel-hady and A. M. Salem, Physica A **242**, 141 (1997).